Medical Engineering and Physics 55 (2018) 9–15

Contents lists available at ScienceDirect

Medical Engineering and Physics

journal homepage: www.elsevier.com/locate/medengphy

Multifractal characteristics of external anal sphincter based on sEMG signals

Paulina Trybek[a,*], Michal Nowakowski[b], Lukasz Machura[a]

[a] Division of Computational Physics and Electronics, Institute of Physics, Silesian Centre for Education and Interdisciplinary Research, University of Silesia, Katowice, Poland
[b] Jagiellonian University School of Medicine, Krakow, Poland

ARTICLE INFO

Article history:
Received 16 May 2017
Revised 5 March 2018
Accepted 13 March 2018

Keywords:
Electromyography
Multifractal analysis
Empirical mode decomposition
Detrended fluctuation analysis

ABSTRACT

Up to 40% of patients treated for rectal cancer suffer from therapy-related symptoms. Innervation injury is one of the suggested pathomechanisms of those symptoms hence the development of a valid, non-invasive tool for the assessment of neural systems is crucial. The aim of this work is to study the fractal properties of the surface electromyography signals obtained from patients suffering from rectal cancer. The anal sphincter activity was investigated for the group of 15 patients who underwent surgical treatment. Multifractal detrended fluctuation analysis was implemented to analyze the data, obtained at four different stages: one before treatment and three times after the surgery. The results from the standard detrended fluctuation analysis and empirical mode decomposition methods are presented and compared. The statistically significant differences between the stages of treatment were identified for the selected spectral parameters: width and maximum of the spectrum.

1. Introduction

Over last few decades, surface electromyography (sEMG), due to its non-invasive characteristics, has gained a wide range of applications for neuromuscular systems. This work is focused on an application of the sEMG concerning the diagnosis of the anal sphincter of the patients suffering from rectal cancer [1,2]. Rectal cancer remains to be one of the most frequent cancers in humans [3]. It requires complex multimodal treatment composed of surgery, irradiation and chemotherapy. All of those methods can cause significant stool continence-related problems hence proper assessment of anorectal innervation before and after the treatment can be crucial for the prevention and treatment of complications. The diagnostics of innervation of the anal sphincter is undeniably a central issue for the evaluation of treatment progress but there is still no practical diagnostic test whose usefulness is scientifically proven. sEMG enables non-invasive monitoring of the anal sphincter function [4–6] and is a very promising method of testing of innervation of muscles.

Regardless of the application, sEMG always represents highly complex signals with a low signal to noise ratio [7]. The nonlinearity of sEMG data has been investigated in recent years [8] and great effort has been devoted to the application of variety of nonlinear methods. Traditional analysis, mainly based on the conventional statistical tests of mean, median or frequency components brings only limited knowledge on the actual process hidden behind the acquired data [9].

In recent years there has been a growing interest in the fractal properties of physiological data and also in the context of sEMG signals [10–12]. This work proposes the application of modified Multifractal Detrended Fluctuation Analysis (MFDFA) based on Empirical Mode Decomposition (EMD) to the sEMG signals. The EMD and MFDFA techniques can be used to trace out the features of non-linear and non-stationary signals. Moreover, both methods have a broad spectrum of applications individually. MFDFA, introduced by Halsey et al. [13] and developed later by Kantelhardt et al. [14] has been used in many disciplines and still attracts considerable attention in the field of physiology, economics, climatology, to name but a few. In relation to electrophysiological signals, MFDFA brought a significant contribution to the analysis of heart rate variability [15,16]. For Empirical Mode Decomposition (EMD) an equally wide range of applications can be found such as the removal of artifacts and noise reduction from the signals [17]. EMD also exhibits better results in the process of detrending in comparison, for example, with the typically used least square method [18]. This aspect has been used in the modified detrending algorithm which is presented in this paper. The use of the EMD method in the context of detrending operations results in a more accurate

* Corresponding author.
E-mail address: paulina.trybek@smcebi.edu.pl (P. Trybek).

https://doi.org/10.1016/j.medengphy.2018.03.007
1350-4533/

trend which is not predetermined and therefore is closely related to the nature of real data [19]. Moreover, it is documented in the literature that this approach outperforms standard MFDFA for large fluctuations [20].

2. Method

2.1. Detrended Fluctuation Analysis (DFA)

The DFA method was first proposed by Peng in 1994 for investigating the correlation in DNA structure [21]. Recent years have seen a renewed importance in the application of this method to biological data and also for distinguishing healthy and pathological states [22]. The basic idea of this technique relies on the assumption that the signal is influenced by the short-term and long-term features. For the proper interpretation of effects hidden behind internal dynamics the signal is analyzed at multiple scales [23]. The brief description of the original DFA algorithm is presented below.

The procedure starts with the calculation of the profile y_i as the cumulative sum of the data x_i with the subtracted mean $\langle x \rangle$:

$$y_i = \sum_{k=1}^{i} [x_k - \langle x \rangle] \tag{1}$$

Next, the cumulative signal y_i is split into N_s equal non-overlapping segments of size s. Here for the length s of the segments we use powers of two, $s = 2^r, r = 4 \ldots 11$. For all segments $v = 1, \ldots, N_s$ the local trend $y^m_{v,i}$ is calculated. In a standard DFA method, the trend is calculated by means of the least-square fit of order m. In this work $m = 2$ was used. The variance F^2 as a function of the segment length s is calculated for each segment v separately.

$$F^2(s, v) \equiv \frac{1}{s} \sum_{i=1}^{s} \left(y^m_{v,i} - y_{v,i} \right)^2. \tag{2}$$

For the last step, the Hurst scaling exponent H is calculated as the slope of the regression line of double-logarithmic dependence, $\log F \sim H \log s$.

2.2. Empirical Mode Decomposition (EMD)

The EMD is an iterative technique which decomposes the signal x(t) into a finite number of Intrinsic Mode Functions (IMFs) $c_i(t)$ and final residual signal $r_n(t)$

$$x(t) = \sum_{i=1}^{n} c_i(t) + r_n(t). \tag{3}$$

The latter can be interpreted as an actual trend. The calculated signal must satisfy two conditions in order to be an IMF: (i) the number of extrema and the number of zero crossings must be equal to or differ at most by one; and (ii) the mean value of the upper and lower envelope defined by local maxima and minima must be zero. The standard EMD method often faces some difficulties, which are recurrently the consequence of signal intermittency referred to as the Mode-Mixing problem. Ensemble Empirical Mode Decomposition (EEMD) [24] and more recent Complete Ensemble Empirical Mode Decomposition (CEEMD) [25] have been proposed in order to overcome this complication. Both methods are based on the averaging over several realizations of Gaussian white noise artificially added to the original signal. For this work however, we use only standard EMD due to the fact that only residual r_n, i.e. the data trend, is needed for further calculations and none of the individual IMFs is considered here explicitly.

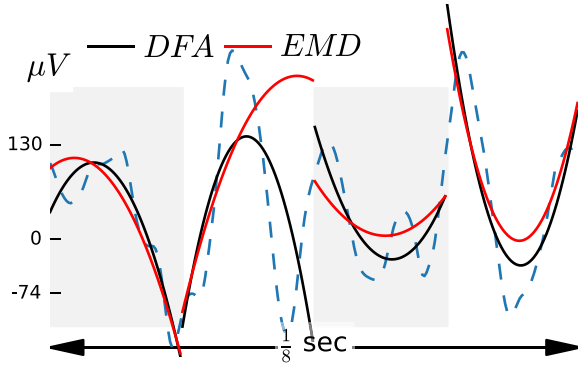

Figure 1. Two detrending methods: DFA (solid black) and EMD (solid red) are presented for the profile y_i of the sEMG example data (dashed blue). (For interpretation of the references to color in this figure legend, the reader is referred to the web version of this article.)

2.3. EMD based DFA

The analysis is now branched into a standard DFA algorithm and non-standard based on EMD techniques. The former method uses the least-square estimation of the order m. The latter utilizes the fact that the residual r_n (3) represents the local trend, thus the standard polynomial fit (DFA) can be replaced by a residuum for each segment [26]. An example of local trends calculated with both methods is presented in Figure 1 for the segment size $s = 64$. The slight differences between solid black and red lines, which represent DFA and EMD methods respectively, influence the further results.

2.4. MFDFA

MFDFA is based on the scaling properties of the fluctuations. The brief description of the method is presented below, however, for detailed specification we suggest works by Kantelhardt et al. [14,27], Ihlen [28] or Salat et al. [29]. In order to extend the monofractal DFA (2.1) to the multifractal DFA it is necessary to indicate the qth statistical moment of the calculated variance (2).

$$F_q(s) = \begin{cases} \left(\frac{1}{2N_s} \sum_{v=1}^{2N_s} [F^2(s, v)]^{\frac{q}{2}} \right)^{\frac{1}{q}}, & q \neq 0, \\ \exp\left\{ \frac{1}{4N_s} \sum_{v=1}^{2N_s} \ln \left[F^2(s, v) \right] \right\}, & q = 0. \end{cases} \tag{4}$$

Next, the determination of the scaling law $F_q(s) \sim s^{h(q)}$ of the fluctuation function (4) is performed with the use of the log–log dependencies of $F_q(s)$ versus segment sizes s for all values of q separately. The q-order Hurst exponent $h(q)$ is required in order to calculate further dependencies. The mass exponent is obtained via the formula

$$\tau(q) = qh(q) - 1. \tag{5}$$

It is then used to calculate a q-order singularity Hölder exponent $\alpha = \tau'(q)$ where the prime means differentiation with respect to the argument. In turn, the q-order singularity dimension can be constructed

$$f(\alpha) = q\alpha - \tau(q) = q[\alpha - h(q)] + 1. \tag{6}$$

The singularity dimension $f(\alpha)$ is related to the mass exponent $\tau(q)$ by a Legendre transform. The multifractal spectrum, i.e. the dependence $f(\alpha)$ vs α is the final result of MFDFA method.

The mf-spectrum describes how often the irregularities of certain degrees occur in the signal. $f(\alpha)$ represent q-order singularity

dimension and α stands for the q-order singularity exponent. The typical monofractal time series has a dense mf-spectrum around the single point ($\alpha = 0, f(\alpha) = 1$). A large difference between periods when small and large fluctuations take place increases, in turn, the width of the spectrum.

In this work, we mainly focus on the two parameters describing the spectrum: width Δ and maximum $\alpha_{\max}$. The width reflects the temporary variation of the local Hurst exponent or the temporal variation of the fractal properties of the fluctuations of the sEMG signal. From the physiological point of view, it can be seen as the quantity which characterizes the temporal fractal variability of the signal, i.e. how the local fractal structures differ from the global Hurst exponent among sEMG signal segments with larger or smaller average fluctuations. Maximum $\alpha_{\max}$ is assigned to the Hurst exponent which appears most frequently in all the examined segments. It describes the location of the most frequent singularity at all scales.

There are two general sources of multifractality which can affect the shape of the mf-spectrum: (i) the broad probability density function which lies behind the data (or its fluctuations); (ii) different behavior of the (auto)correlation function for large and small fluctuations. Furthermore, both situations are possible simultaneously. Simple data shuffling can test the possible source of multifractality. In case (i) shuffling will not change the mf-spectrum, for (ii) it will destroy the effect completely as the shuffling will erase the possible correlations. In the case of (i) and (ii) present simultaneously the spectrum will differ from the original one as the shuffled series will exhibit somehow weaker multifractality [30].

3. Material

3.1. sEMG signal source

Data acquisition system consists of an anal probe developed at the Laboratory of Engineering of Neuromuscular System and Motor Rehabilitation of Politecnico di Torino in collaboration with the company OT-Bioelettronica. Signals were obtained from 16 pairs of silver bar electrodes of length 9 mm and width 1 mm each. Electrodes were separated by 8 mm and arranged concentrically at three levels 35–44 mm, 18–27 mm and around 9 mm of rectal canal depth from the anal verge. The probe worked in conjunction with the standard PC over a 12-bit NI DAQ MIO16 E-10 transducer (National Instruments, USA). The sampling frequency was 2048 Hz, which for the 10 s of the measurement gave 20480 data points. Low and high pass filters were used at 10 and 500 Hz respectively. This resulted in a typical 3 dB bandwidth for the Analogue-to-Digital Converter. The analyzed time series were recorded at four stages: before the treatment (D_1) and one month (D_2), 6 months (D_3) and 1 year (D_4) after the surgical procedure. The detailed information about the surgery for rectal cancer and the role of sEMG for the patient diagnosis can be found in [31].

Measurement protocol included, consecutively, a 1-min relaxation state; three 10 s recordings at rest; a 1-min relaxation and; three 10 s recordings at maximum voluntary contraction (MVC). Each signal was recorded at three levels of anal canal depth, respectively 5 cm, 3 cm and 1 cm. For our calculations, signal recordings during voluntary contraction at the depth of 1 cm were used. This specific choice of depth was dictated by the maximal amplitude of the EMG signal resulting from the most superficial localization of external anal sphincter muscle and the biggest bulk of the muscle at this location. Figure 2 presents an example of the raw signals at four stages of rectal cancer treatment. For better visualization of the character of a waveform, a narrow range of time scale is presented. The difference in the amplitude values between the state directly after operation (D_2) and the rest of states (D_1, D_3, D_4) is visible to the naked eye. One month after the operation the values of amplitude are respectively lower in comparison with other stages. The signal used in this work is, in fact, the averaged signal from the first 3 channels which corresponds to the first three pairs of the electrodes. The nearest neighbors average was performed due to the fact that the placement of the probe in subsequent measurements could be inaccurate. In other words, the specific electrodes may not be located exactly the same place at the consecutive measurements after the surgery.

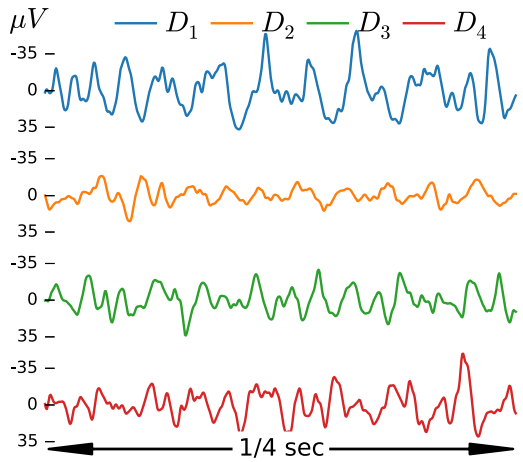

Figure 2. The raw signals truncated to 1/4 of the second at four stages of rectal cancer treatment: D_1 is assigned to the state before surgery, D_2 – D_4 correspond to 1 month, 6 months and 1 year after the surgery, respectively.

3.2. Patients

The study included 15 subjects, 5 females of age range 46 to 71 (average 53.4 years) and 10 males of age range 40 to 85 (average 62.8 years) diagnosed with rectal cancer and qualified for surgery. Based on the localization of the rectal cancer, patients underwent either Low Anterior Resection (LAR, 9 patients), Anterior Resection (AR, 5 patients) or proctocolectomy (PC, 1 patient).

4. Results

4.1. Fluctuation analysis

Clearly, MFDFA is not a black-box method and always requires some individual decisions. First of all, the choice of the scaling range can have a significant impact on the appropriate estimation of the fluctuation function (F_q) and consequently the final results [16,28]. For the calculations presented in this work, the considered range of scales are between $s \in [2^4, 2^{11}]$. The parameter q should consist of positive and negative values in order to detect periods with small and large fluctuations [28]. In our case $q \in [-5, 5]$ were chosen. A set of q-order fluctuation functions F_q vs segment size s is presented in Figure 3. The two different scale ranges are clearly visible for all $F_q(s)$ characteristics. This bisection into two distinct scaling regimes plays a crucial role in the determination of the q-order Hurst exponent $h(q)$ and therefore impacts the further analysis. The results for DFA (+) and EMD-based (×) detrending methods are presented in Figure 3. Two separate scaling domains was accepted, namely $s \in [2^4, 2^6]$ and $s \in [2^8, 2^{11}]$. Further analysis has been performed for both of these regions separately. The middle values $s \in (2^6, 2^8)$ are omitted, as there is no clear linear scaling present.

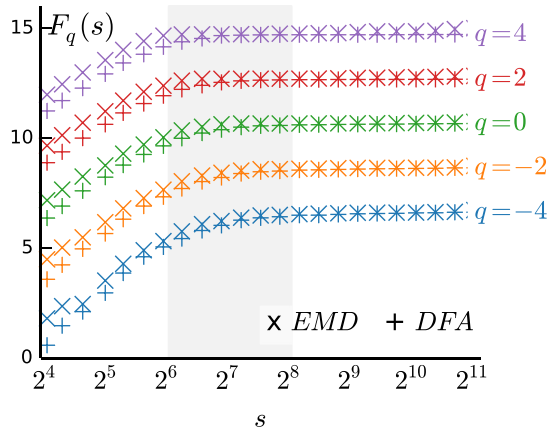

Figure 3. q-th order fluctuation function (4) with both detrending methods DFA of order 2 and EMD presented for data before the surgery D_1 for selected values of q. Characteristics were artificially shifted vertically for better visibility.

4.2. Multifractal spectra

The central result of this work is presented in Figure 4. It sets together the multifractal spectra at all levels of the treatment process ($D_1 - D_4$). Each graph includes spectra calculated by both DFA and EMD detrending methods for small and large ranges of scales separately. Additionally, the spectra obtained after shuffling operations are presented on each individual chart. For all of the examined cases, the relatively wide spectra for the short scales $s < 2^6$ can be observed. For the large scales, $s > 2^8$ the small set of points located at (0, 1) is visible. This indicates the multifractal character of the sEMG signal for the short scales $s < 2^6$ and a rather monofractal character for the large scales $s > 2^8$. For all of the presented analyses, regardless of the method, the spectra calculated for the small scaling region $s < 2^6$, exhibit long right tails, see Figure 4. This means that the multifractal structure is sensitive to the local fluctuations with small magnitudes on the short time scales only [28]. On the comparison of the spectra obtained by the two methods, a shift toward the smaller values of α (left side) of the spectrum for the small scales $s < 2^6$ is visible for all signals in the case of the EMD-based MFDFA.

The spectra calculated for the shuffled data (see black line in Figure 4) form a tight set of points, significantly shifted toward the lower values of singularity exponent α. In other words, the shuffling operation resulted in a complete destruction of multifractality which occurs for the raw data. Thus it can be concluded that multifractal character of the raw data has its cause in different behavior of the correlation function for large and small fluctuations.

Table 1
Average values of the spectrum width $\langle\Delta\rangle$ and maximum of spectrum α_{max} together with the standard deviations presented for all channels at each state of the treatment D_1 – D_4. Results are presented for the MFDFA and EMD-based MFDFA methods.

Average spectrum width $\langle\Delta\rangle$ for $s < 2^6$				
	D_1	D_2	D_3	D_4
DFA	0.981 ± 0.362	0.950 ± 0.342	1.053 ± 0.418	0.967 ± 0.355
EMD	0.848 ± 0.316	0.808 ± 0.310	0.880 ± 0.350	0.812 ± 0.307
Average spectrum width $\langle\Delta\rangle$ for $s > 2^8$				
DFA	0.136 ± 0.068	0.142 ± 0.052	0.130 ± 0.055	0.161 ± 0.118
EMD	0.107 ± 0.070	0.112 ± 0.053	0.100 ± 0.054	0.131 ± 0.118
Maximum of the spectrum α_{max} for $s < 2^6$				
DFA	1.580 ± 0.107	1.577 ± 0.117	1.588 ± 0.110	1.593 ± 0.104
EMD	1.405 ± 0.098	1.414 ± 0.100	1.414 ± 0.096	1.423 ± 0.089
Maximum of the spectrum α_{max} for $s > 2^8$				
DFA	0.030 ± 0.011	0.031 ± 0.008	0.031 ± 0.012	0.031 ± 0.009
EMD	0.017 ± 0.009	0.017 ± 0.007	0.017 ± 0.010	0.017 ± 0.008

4.3. Statistics of spectral parameters

Table 1 summarizes the average values of the spectrum width $\langle\Delta\rangle$ and the specific singularity exponent $f(\alpha_{max}) = 1$ which corresponds to the maximum of the spectrum calculated for all of the analyzed cases and the whole set of 16 electrodes at each treatment state.

The location of the maximum of the spectrum is always found for the greater values of the singularity exponent in the case of standard MFDFA method. Also the width of the spectrum is consistently wider for the standard MFDFA. The shift toward the higher values of spectrum parameters for the standard MFDFA is also visible on the presented histograms, see Figure 5. The differences are more evident in the graphs that characterize the maximum of the spectrum for both small and large ranges of scales. The normality tests of presented probability distributions by means of the Shapiro–Wilk formula do not allow us to reject the hypothesis of normality for some selected cases. At the chosen significance level $\alpha = 0.05$, p-value is always greater than α for both the spectrum width and the maximum of the spectrum for the small scaling range ($s < 2^6$) at the state one month after the surgical procedure ($D2$). Additionally, the same results were obtained for the state one year after the operation ($D4$) for the maximum of the spectrum only however.

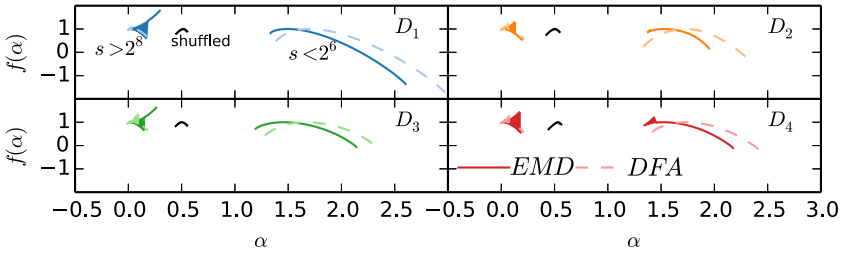

Figure 4. An example of multifractal spectra calculated for one case at four stages of rectal cancer treatment D_1 – D_4. At each panel, three sets of distinct spectra can be found: right corresponds to the scaling region $s < 2^6$, the middle represents the whole range of scales $s \in [2^4, 2^{11}]$ after the shuffling operation and left set for $s > 2^8$. For each scaling regions, two spectra are presented—the EMD based MFDFA (dark solid lines) and standard MFDFA (light dashed lines). In the case of shuffled data, the spectra calculated by both methods are overlapped almost entirely. One may notice the generally found degeneracy of the spectra for $s > 2^8$ and the shift toward the smaller values of α for the EMD-based detrending.

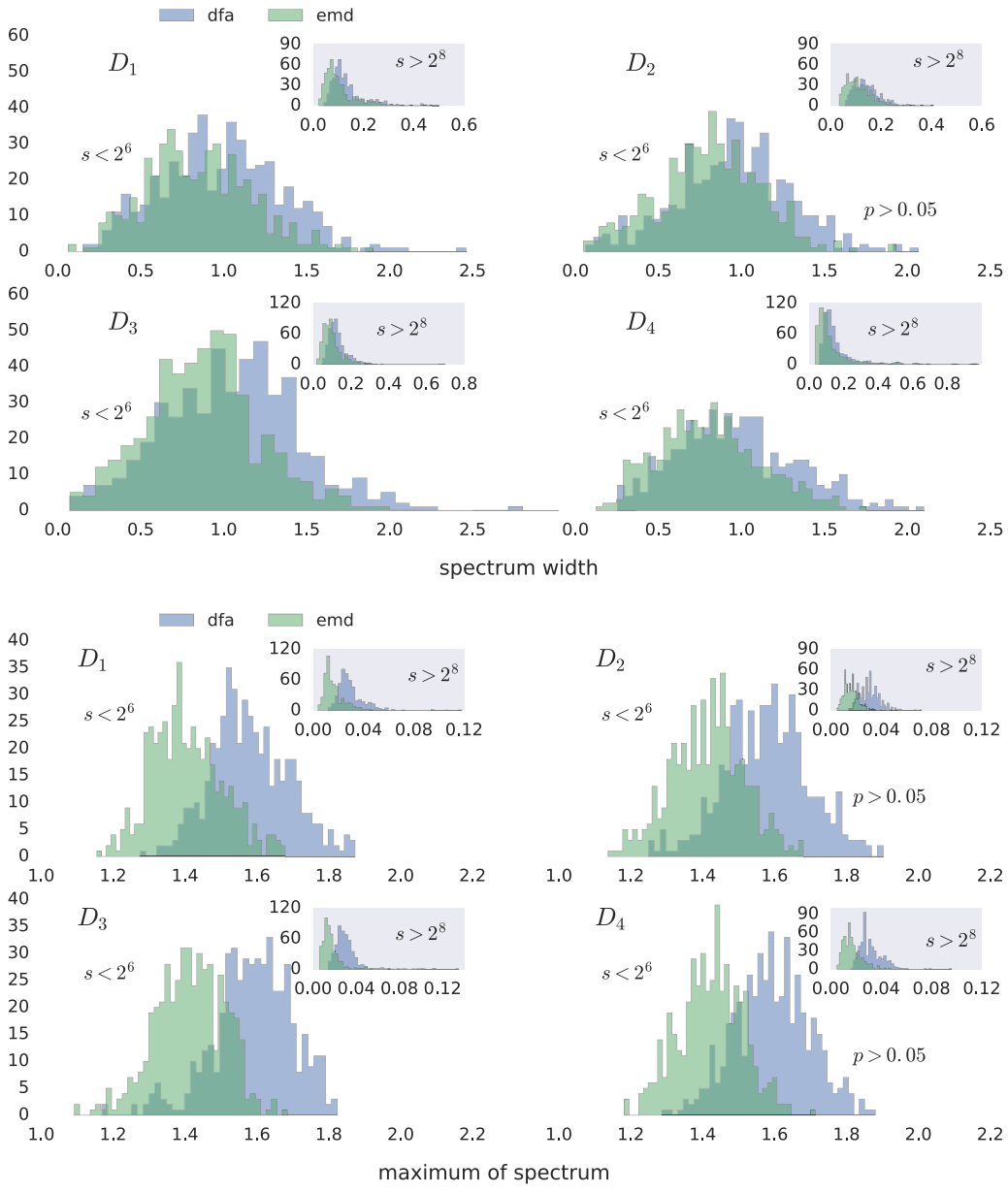

Figure 5. The probability distributions of spectral parameters calculated for both EMD and DFA methods at each stage of treatment: large histograms represent the small scaling region $s < 2^6$; the insets stand for the histograms corresponding to the large range of scales.

Figure 6 presents the box plot of spectral parameters calculated for the small scaling region $s < 2^6$. The comparison of mf-spectrum parameters calculated by the DFA method for different stages of treatment show a decrease in the average value of the spectrum maximum α_{max} and spectrum width $\langle\Delta\rangle$ for the state one month after the surgery—$D2$ and re-growth for the next state. It is noticeable that in the case of a maximum $\alpha_{\max}$ the results for D_2 obtained by both methods are ambiguous. In contrast to the DFA technique, we observe the increase of the mean value of a maximum of the spectrum for the EMD method. In order to identify the differences between individual stages of treatment, the Friedman test has been applied. It is a widely known non–parametric equivalent of the one-factor analysis of variance for repeated measurements. The values of ANOVA χ^2, Kendall's coefficient of concordance and the p-values are presented in Table 2. The values highlighted in bold are assigned to a statistical significance of the difference between four comparing stages (D_1, D_2, D_3, D_4) at the selected significance level $\alpha = 0.05$. Statistically significant differences between compared stages can be found for all parameters except the maximum of spectrum calculated by the DFA method in the small scales regime.

Table 2
The results of non-parametric Friedman test calculated for spectral parameters.

	Spectrum width(Δ)		Max. of spectrum($\alpha_{\max}$)	
	DFA	EMD	DFA	EMD
$s < 2^6$				
Anova χ^2	17.178	18.365	7.254	10.104
Kendall coeff.	0.012	0.013	0.005	0.007
p-value	**0.001**	**0.000**	0.064	**0.018**
$s < 2^8$				
Anova χ^2	43.920	35.4968	41.614	12.878
Kendall coeff.	0.031	0.025	0.029	0.009
p-value	**0.000**	**0.000**	**0.000**	**0.005**

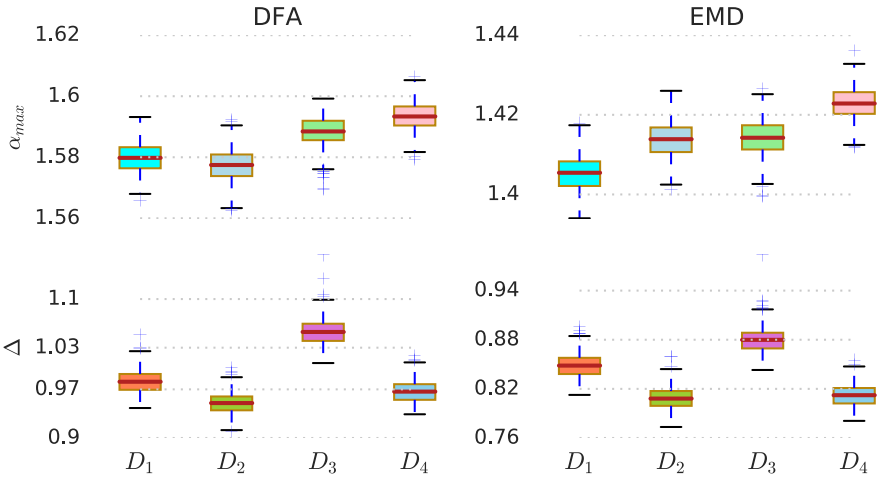

Figure 6. The box plots present the average values of spectral parameters with the standard error of the mean. The maximum of the spectrum and its width calculated by the DFA method are shown on two diagrams on the l.h.s. in contrast to the EMD results presented in the right column.

5. Discussion

This work tests the multifractal character of the sEMG signals recorded from an external anal sphincter at different stages of rectal cancer treatment procedure. For each analyzed time series, two distinct scaling regions were identified for which multifractal spectra exhibit a different character. The multifractal and monofractal nature can be seen in the regions of the short and large time scales respectively. Additionally, the multifractal spectra based on the standard DFA were compared with the EMD based one. The latter algorithm shifts the spectra toward the higher fluctuations or smaller values of the singularity exponent. The average values of the considered spectral parameters (width and maximum) for individual stages of treatment are respectively lower in the EMD case. This seems to be the generic behavior for the analyzed EMG data. The changes of parameters between individual stages, D_1–D_4, has exactly the same tendency when the results of those two methods are compared. Additionally, the source of multifractality within the short timescales was identified as a result of the long-range correlation effects for large and weak fluctuations. The statistical analysis of spectral parameters with the non-parametric Friedman ANOVA indicates the occurrence of statistically significant differences between individual stages of treatment in the case of spectral width for both detrending methods—DFA and EMD. Applied fractal methods also show the decreasing spectrum width one month after the surgical operation for all of the patients. Some limitation of this study is related to the medical aspect of our research and concerns the problem of a relatively low number of subjects. In a small group of patients, we observe relatively large heterogeneity. Some of the obtained results might gain significance along with an increasing number of subjects hence more experimental work will be needed to verify more accurate variability of spectral parameters among the individual stages of treatment.

Although an experimental part of this work is still at an early stage of development, it can be seen as a procedure which brings a new understanding of the properties of the sEMG signals. There is a constant need for the assessment of new nonlinear parameters and methods for a better physiological understanding of the nature of bio–medical signals. Multi-fractal description can serve as a powerful tool in order to do that.

Acknowledgments

Authors would like to thank Karina Maciejewska for fruitful discussions and Andrew Watson for a proofreading of this manuscript.

Conflicts of interest

None

Funding

This work was partially supported by the JUMC research grant: K/ZDS/006369.

Ethical approval

Research was approved by a decision of Bioethical Committee of Jagiellonian University for research grant WL-ZKL-94.

References

[1] Nowakowski M, Tomaszewski KA, Herman RM, Sałówka J, Romaniszyn M, Rubinkiewicz M, Walocha JA. Developing a new electromyography-based algorithm to diagnose the etiology of fecal incontinence. Int J Colorectal Dis 2014;29(6):747–54.
[2] Merletti R, Bottin A, Cescon C, Farina D, Gazzoni M, Martina S, Mesin L, Pozzo M, Rainoldi A, Enck P. Multichannel surface EMG for the non-invasive assessment of the anal sphincter muscle. Digestion 2004;69(2):112–22.
[3] Bray F, Jemal A, Grey N, Ferlay J, Forman D. Global cancer transitions according to the human development index 2008–2030: a population-based study. Lancet Oncol 2012;13(8):790–801.
[4] Enck P, Hinninghofen H, Merletti R, Azpiroz F. The external anal sphincter and the role of surface electromyography. Neurogastroenterol Motil 2005;17(s1):60–7.
[5] Kauff DW, Wachter N, Heimann A, Kruger TB, Hoffmann KP, Lang H, Kneist W. Surface electromyography reliably records electrophysiologically evoked internal anal sphincter activity: a more minimally invasive approach for monitoring extrinsic innervation. Eur Surg Res 2016;57(1–2):81–8.
[6] Cescon C, Mesin L, Nowakowski M, Merletti R. Geometry assessment of anal sphincter muscle based on monopolar multichannel surface EMG signals. J Electromyogr Kinesiol 2011;21(2):394–401.
[7] Clancy E, Morin EL, Merletti R. Sampling, noise-reduction and amplitude estimation issues in surface electromyography. J Electromyogr Kinesiol 2002;12(1):1–16.
[8] Lei M, Wang Z, Feng Z. Detecting nonlinearity of action surface EMG signal. Phys Lett A 2001;290(5):297–303.
[9] Stanley H, Amaral LN, Goldberger A, Havlin S, Ivanov PC, Peng CK. Statistical physics and physiology: monofractal and multifractal approaches. Physica A 1999;270(1):309–24.
[10] Goldberger AL, Amaral LA, Hausdorff JM, Ivanov PC, Peng CK, Stanley HE. Fractal dynamics in physiology: alterations with disease and aging. Proc Natl Acad Sci 2002;99(Suppl 1):2466–72.
[11] Atupelage C, Nagahashi H, Yamaguchi M, Sakamoto M, Hashiguchi A. Multifractal feature descriptor for histopathology. Anal Cell. Pathol 2012;35(2):123–6.
[12] Wang G, Ren XM, Li L, Wang ZZ. Multifractal analysis of surface EMG signals for assessing muscle fatigue during static contractions. J Zhejiang Univ—Sci A 2007;8(6):910–15.
[13] Halsey TC, Jensen MH, Kadanoff LP, Procaccia I, Shraiman BI. Fractal measures and their singularities: the characterization of strange sets. Phys Rev A 1986;33:1141–51.

[14] Kantelhardt JW, Zschiegner SA, Koscielny-Bunde E, Havlin S, Bunde A, Stanley HE. Multifractal detrended fluctuation analysis of nonstationary time series. Physica A 2002;316(1):87–114.
[15] Makowiec D, Rynkiewicz A, Gałaska R, Wdowczyk-Szulc J, Żarczyńska-Buchowiecka M. Reading multifractal spectra: aging by multifractal analysis of heart rate. EPL (Europhys Lett) 2011;94(6):68005.
[16] Gierałtowski J, Żebrowski J, Baranowski R. Multiscale multifractal analysis of heart rate variability recordings with a large number of occurrences of arrhythmia. Phys Rev E 2012;85(2):021915.
[17] Andrade AO, Nasuto S, Kyberd P, Sweeney-Reed CM, Kanijn FV. EMG signal filtering based on empirical mode decomposition. Biomed Signal Process Control 2006;1(1):44–55.
[18] Liu D, et al. Precipitation complexity measurement using Multifractal spectra empirical mode decomposition Detrended fluctuation analysis. Water Resour Manage 2016;30(2):505–22.
[19] Yeh JR, Fan SZ, Shieh JS. Human heart beat analysis using a modified algorithm of detrended fluctuation analysis based on empirical mode decomposition. Med Eng Phys 2009;31(1):92–100.
[20] Qian XY, Gu GF, Zhou WX. Modified detrended fluctuation analysis based on empirical mode decomposition for the characterization of anti-persistent processes. Physica A 2011;390(23):4388–95.
[21] Peng CK, Buldyrev SV, Havlin S, Simons M, Stanley HE, Goldberger AL. Mosaic organization of DNA nucleotides. Phys Rev E 1994;49(2):1685.
[22] Rodriguez E, Echeverria JC, Alvarez-Ramirez J. Detrended fluctuation analysis of heart intrabeat dynamics. Physica A 2007;384(2):429–38.
[23] Semmlow JL, Griffel B. Biosignal and medical image processing. CRC Press; 2014.
[24] Wu Z, Huang NE. Ensemble empirical mode decomposition: a noise-assisted data analysis method. Adv Adapt Data Anal 2009;1(1):1–41.
[25] Torres ME, Colominas MA, Schlotthauer G, Flandrin P. A complete ensemble empirical mode decomposition with adaptive noise. In: 2011 IEEE international conference on acoustics, speech and signal processing (ICASSP), IEEE; 2011. p. 4144–7.
[26] Caraiani P. Evidence of multifractality from emerging European stock markets. PLoS One 2012;7(7):e40693.
[27] Kantelhardt JW. Fractal and multifractal time series. In: Mathematics of complexity and dynamical systems. Springer; 2012. p. 463–87.
[28] Ihlen Espen Alexander Fürst EAFI. Introduction to multifractal detrended fluctuation analysis in Matlab. Front physiol 2012;3:141.
[29] Salat H, Murcio R, Arcaute E. Multifractal methodology. Physica A: Statistical Mechanics and its Applications 2017;473:467–87.
[30] Horvatic D, Stanley HE, Podobnik B. Detrended cross-correlation analysis for non-stationary time series with periodic trends. EPL (Europhys Lett) 2011;94(1):18007.
[31] Delaini GG, Scaglia M, Colucci G, Hultén L. Functional results of sphincter-preserving operations for rectal cancer. In: Rectal cancer. Springer; 2005. p. 147–55.